Magnetically Induced Vibrations in an IPM Motor Due to Distorted Magnetic Forces Arising From Flux Weakening Control

D. Y. Kim, G. H. Jang, and J. K. Nam

PREM Lab, Department of Mechanical Engineering, Hanyang University, Seoul 133-791, Korea

This research investigates the characteristics of magnetic forces and magnetically induced vibrations due to changes in the phase angle of applied current arising from flux weakening control of an interior permanent magnet (IPM) motor. The magnetic force is analyzed using the Maxwell stress tensor method, and the vibration induced by the application of a rotating magnetic force is analyzed using the mode superposition method. The experiments are conducted to validate the simulated vibrations due to the distorted magnetic forces. This research shows that flux weakening control may increase the magnetically induced vibration due to increases in tangential magnetic forces.

***Index Terms*—Flux weakening control, interior permanent magnet (IPM) motor, magnetic force, magnetically induced vibration.**

I. Introduction

INTERIOR PERMANENT MAGNET (IPM) motors, due to their high torque output and a wide operating speed range, have recently made their way into many varied industry applications such as home appliances and electric vehicles. The high torque output is obtained by the use of both electromagnetic and reluctance torques; a wide operating speed range is achieved with flux weakening control, which decreases the back electromagnetic motive force (BEMF) by applying a negative d-axis current, as shown in Fig. 1.

Many researchers have investigated flux weakening control. Jahns and Kim *et al.* investigated an algorithm for flux weakening control that is independent of motor parameters and operating conditions [1], [2]. Zhu *et al.* showed that the iron loss of IPM motors is larger than that of SPM motors even though IPM motors have a structure suitable for flux weakening control due to their high demagnetization characteristics [3]. Kim *et al.* investigated the forced vibration of a stator by the application of magnetic force [4]. However, they did not consider tangential magnetic forces and vibrations caused by current variations. Jiao *et al.* investigated flux weakening control to reduce radial force [5]. They also characterized the radial magnetic force according to varying d-axis current; they did not, however, consider tangential magnetic forces and magnetically induced vibration. The control algorithms and performance of flux weakening control have been studied by several researchers, but the characteristics of magnetic force and the vibration caused by variation in the current have not yet been investigated. No research has been reported on distorted magnetic forces and the magnetically induced vibrations caused by flux weakening control.

This research investigates the characteristics of both radial and tangential magnetic forces acting on the teeth of a stator as well as the magnetically induced vibrations of a spoke-type IPM motor under flux weakening control, shown in Fig. 2, according to variations in the phase angle of applied current (β). The magnetic force is calculated by the 2-D magnetic finite element (FE) method and the Maxwell stress tensor method. The vibration of the motor due to the rotating magnetic force is calculated by the 3-D structural FE method and the mode superposition method. The simulated result is validated by experiments in which the phase angle of the applied current was varied.

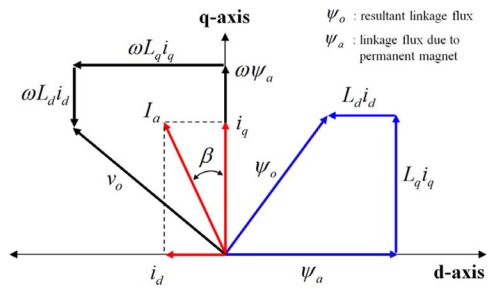

Fig. 1. Vector diagram in dq-axis reference frame.

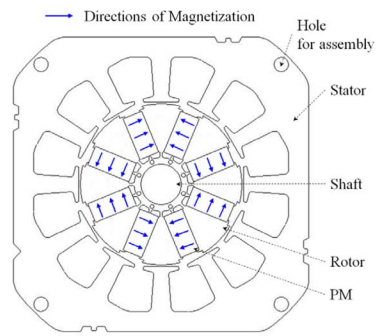

Fig. 2. Structure of a spoke-type IPM motor with 8 poles and 12 slots.

II. Finite Element Analysis

A. Analysis of Magnetic Force

The phase current in motor windings under flux weakening control is determined from the following:

$$i_a = I_a \sin(p\,\omega\, t + \beta) \tag{1}$$

Manuscript received October 28, 2012; accepted January 03, 2013. Date of current version July 15, 2013. Corresponding author: G. H. Jang (e-mail: ghjang@hanyang.ac.kr).

Color versions of one or more of the figures in this paper are available online at http://ieeexplore.ieee.org.

Digital Object Identifier 10.1109/TMAG.2013.2238614

where p, ω, and β are the number of pole pairs, the rotating speed, and the phase angle of the applied current, respectively. The relationship between β, i_d, i_q, and I_a shown in Fig. 1 is as follows:

$$\beta = \tan^{-1}(i_d/i_q) \tag{2}$$

$$I_a = \sqrt{i_d^2 + i_q^2}. \tag{3}$$

A 2-D magnetic FE model of the spoke-type IPM motor with 8 poles and 12 slots, shown in Fig. 2, was developed to calculate the distribution of the magnetic flux density in the air gap. The FE model has 98,643 elements. The magnetic force acting on the teeth is calculated from the magnetic flux density of the air gap using the Maxwell stress tensor method. The radial and tangential magnetic force densities are defined by the following equation [6]:

$$f_{\text{radial}} = \frac{1}{2\mu_{air}}\left(B_r^2 - B_t^2\right) \tag{4}$$

$$f_{\text{tangential}} = \frac{1}{\mu_{air}} B_r B_t \tag{5}$$

where μ_{air} is the permeability of air, and B_r and B_t are the magnetic flux densities in the radial and tangential directions, respectively.

Fig. 3 shows the variation of radial and tangential magnetic force in a motor running at 15,246 RPM with a rotor eccentricity of 25 μm, a phase current of 2.51 A, and a phase angle of 72 degrees as the rotor rotates 90 degrees. The radial magnetic force is distributed along the tooth, but the tangential magnetic force is concentrated on the tooth edge itself. The tangential magnetic force on the left edge is bigger than that on the right edge and generates the magnetic torque in the motor. The torque is defined by the following equation:

$$T = \oint r \times f_{\text{tangential}}\, d\theta. \tag{6}$$

Fig. 4 shows the simulated frequency spectrum of the radial magnetic force acting on a tooth center. The 8th harmonics are major components of the magnetic force because the magnetic force repeats every 45 degrees, as shown in Fig. 3(a). The rotor eccentricity also generates additional harmonics.

The magnetic force is also investigated according to variations in the phase angle of the applied current. In this research, the q-axis current was kept constant to generate constant torque and the d-axis current changed to control the phase angle of the applied current. Fig. 5(a) shows that the radial magnetic force decreases according to increases in the phase angle of the applied current. Figs. 5(b) and 6 show that the tangential magnetic force and the torque ripple increase with increasing phase angle; this is because increases in phase angle of the applied current change the magnetic flux in the air gap to flow easily in a tangential direction. The increased tangential magnetic force proportional to the increase in phase angle of the applied current explains the torque ripple increase as the phase angle between applied current and BEMF increases.

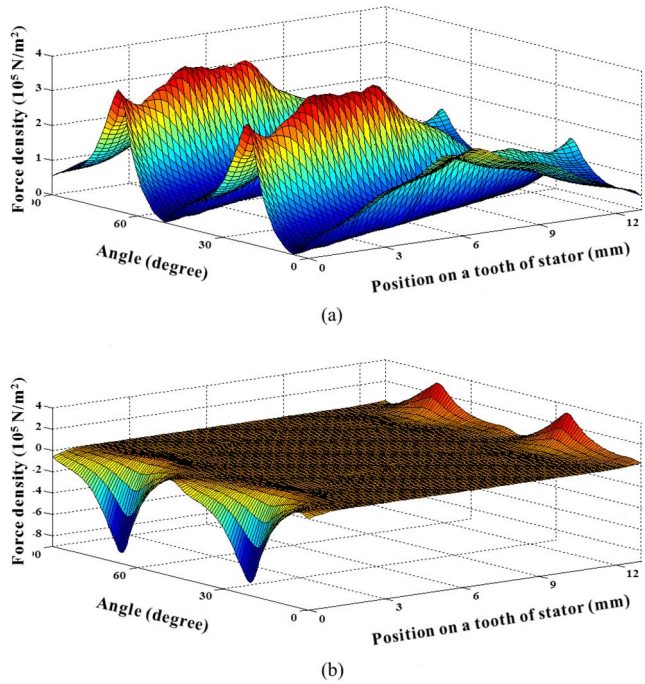

Fig. 3. Simulated (a) radial and (b) tangential magnetic force densities according to spatial position and angle.

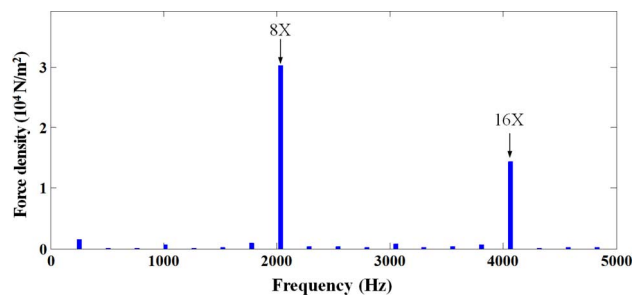

Fig. 4. Simulated frequency spectrum of the radial magnetic force acting on the center of a tooth.

B. Analysis of Magnetically Induced Vibrations

The 3-D structural FE model shown in Fig. 7 was developed to simulate the vibrations induced by the magnetic force. The FE model has 233,786 elements consisting of tetrahedral and brick elements. The elastic modulus E_z and shear moduli G_{xz}, G_{yz} of the stator are much smaller than that of the isotropic material because the stator has a stacked laminated structure [7]. Thus, we make use of its orthotropic property to represent the actual mechanical properties of the stator [8]. The developed FE model of the stator is validated by comparing the simulated natural frequencies with the measured ones via modal testing, the results of which are shown in Table I. The vibrations due to the application of the magnetic force are determined from the following equation:

$$[M]\{\ddot{x}\} + [C]\{\dot{x}\} + [K]\{x\} = \{f_{eq}\} \tag{7}$$

where $[M]$, $[C]$, $[K]$, $\{x\}$, and $\{f_{eq}\}$ are the mass matrix, the damping matrix, the stiffness matrix, the nodal displacement vector, and the equivalent nodal force vector, respectively. $[C]$ is

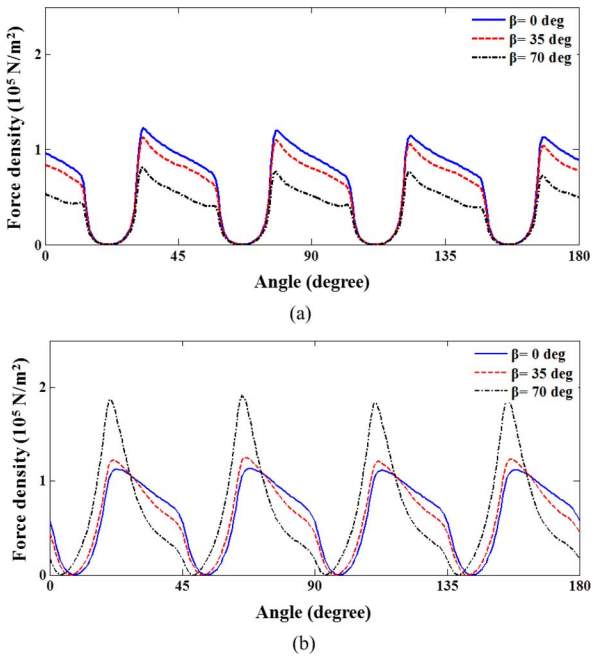

Fig. 5. Simulated magnetic force densities according to variations in the phase angle of the applied current: (a) radial magnetic force on the center of a tooth, (b) tangential magnetic force on the left edge of a tooth.

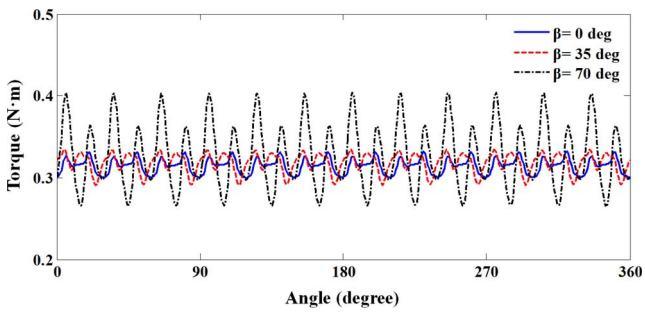

Fig. 6. Simulated torque according to variations in the phase angle of the applied current.

determined from measured modal damping ratios. The vibration of the motor is calculated by the mode superposition method, represented by the following equation:

$$\{x\} = \sum_{i=1}^{N} \{\varphi_i\} y_i \tag{8}$$

where φ_i, y_i, and N are the i-th mode shape, the modal displacement, and the number of mode shapes used in FE analysis, respectively. The thirty mode shapes are superposed to calculate the acceleration after convergence was ensured.

The axial magnetic force is not included because the housing is made of aluminum and there is no overhang between the stator and the rotor to generate axial magnetic forces. Fig. 8 shows the radial acceleration due to the magnetic force on point A shown in Fig. 7. The pole harmonics (eighth and 16th) are the major components of the vibration, and the tenth harmonic (2

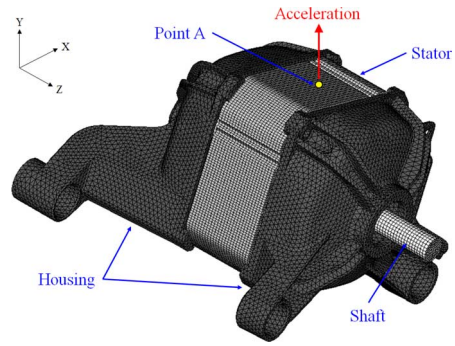

Fig. 7. 3-D finite element model composed of housing, shaft and stator.

TABLE I
COMPARISON OF SIMULATED NATURAL FREQUENCIES OF THE STATOR AND EXPERIMENTAL ONES

Natural frequency (Hz)	1st mode	2nd mode	3rd mode
Simulation	1125	1328	1595
Experiment	1050	1330	1560

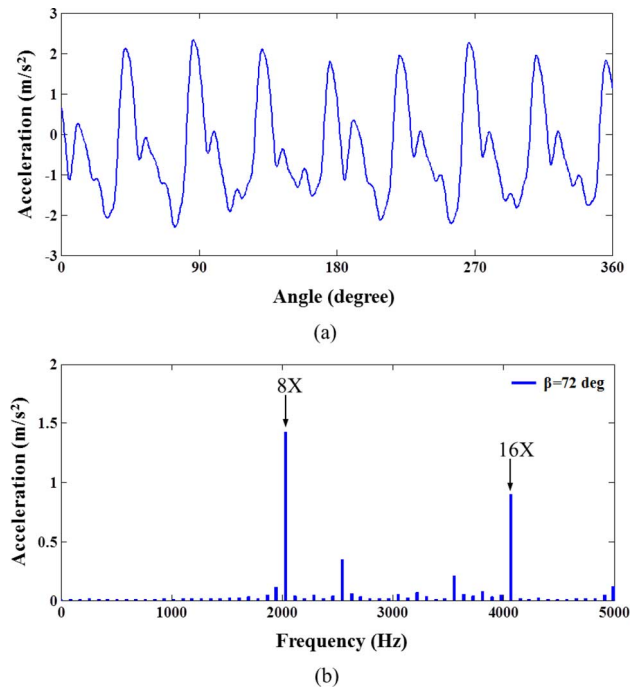

Fig. 8. Simulated radial acceleration on point A of the stator due to magnetic force: (a) time (b) frequency.

540 Hz) originates from the rotor eccentricity and its structural resonance.

The magnetically induced vibration is shown in Fig. 9, plotted against the phase angles of the applied current between 0 and 70 degrees. The magnetically induced vibration decreases as the radial magnetic force decreases, as shown in Fig. 5(a); however, it begins to increase again at a phase angle of approximately 60 degrees because of the influence of the rapidly increasing tangential magnetic force shown in Fig. 5(b). As previous researchers have suggested, the simulated radial magnetic force decreases

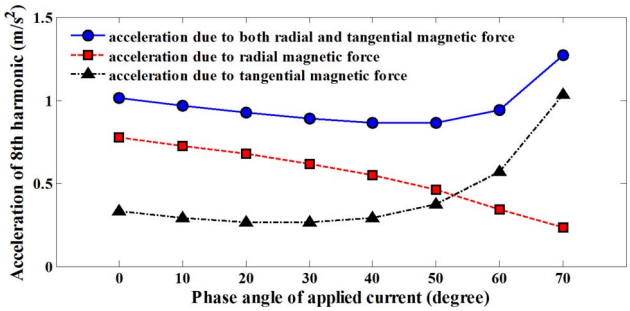

Fig. 9. Simulated acceleration of the 8th harmonic according to changing the phase angle of the applied current.

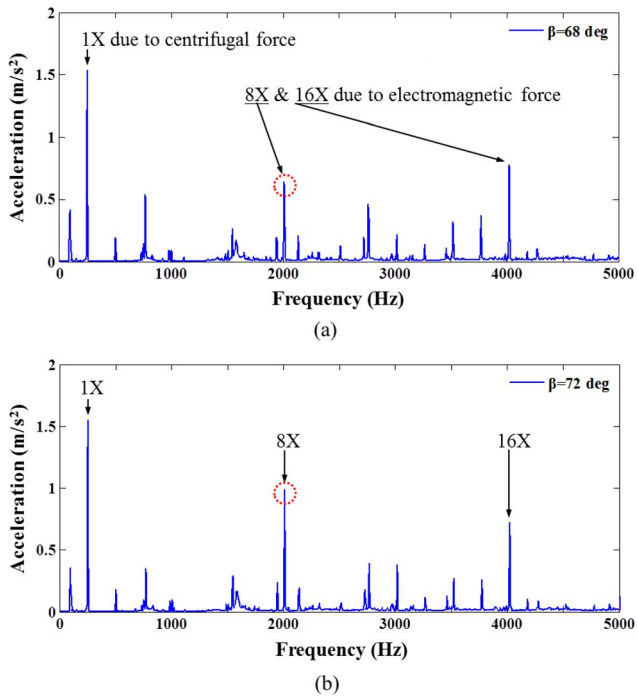

Fig. 10. Measured frequency response of radial acceleration on point A of the stator at a phase angle of the applied current of (a) 68 degrees (b) 72 degrees.

with increases in the phase angle of the applied current. However, the magnetically induced vibration could also increase by the increase of the phase angle of the applied current.

III. Experimental Verification

Experiments are conducted to validate the simulated magnetically induced vibrations due to the distortion of the magnetic force arising from the flux weakening control. The phase angle of the applied current is controlled by the change of the input voltage of the inverter via an automatic voltage regulator (AVR). The input voltage is varied between 220 and 270 V using the AVR. The phase angle is decreased by decreases in the negative d-axis current as the input voltage of the inverter is increased. The acceleration is measured with an accelerometer on point A of the stator, as shown in Fig. 7.

Fig. 10 shows the measured radial acceleration of the motor. One of major excitation sources is the centrifugal force due to the unbalanced mass of the rotor, which generates the first harmonic, but the FE model does not include the centrifugal force, so the first harmonic is not observed in the simulated acceleration shown in Fig. 8(b). The frequency response of the simulated acceleration in Fig. 8(b) matches well with that of the measured acceleration in Fig. 10(b) except for the lack of the first harmonic. The overall level of the measured acceleration decreases from 3.25 to 2.95 m/s^2 when the phase angle of the applied current decreases from 72 degrees at 220 V to 68 degrees at 270 V. The measured dominant acceleration of the 8th harmonic due to the magnetic force decreases by 35% from 0.98 to 0.64 m/s^2, and the simulated one decreases by 27% from 1.43 to 1.03 m/s^2. This experiment validates the simulated result, showing that magnetically induced vibrations may increase with increases in the phase angle of the applied current under flux weakening control.

IV. Conclusion

This research investigates the effects of variation of the phase angle of the applied current under flux weakening control on magnetic force acting on the stator teeth and the magnetically induced vibration of a motor. The radial magnetic force decreases with increasing the phase angle of the applied current but the tangential magnetic force increases. The magnetically induced vibration could increase when the effect of the tangential magnetic force begins to overtake that of the radial magnetic force. The simulated magnetically induced vibrations are validated by experiments. It shows that the use of flux weakening control could increase magnetically induced vibrations because of increases in the tangential magnetic force. This research will contribute to electromagnetic design and flux weakening control strategies to reduce the magnetically induced vibration of IPM motors.

Acknowledgment

This research was supported by Samsung Electronics Co. Ltd.

References

[1] T. M. Jahns, "Flux-weakening regime operation of an interior permanent magnet synchronous motor drive," *IEEE Trans. Ind. Appl.*, vol. IA-23, no. 4, pp. 681–689, 1987.

[2] J. M. Kim and S. K. Sul, "Speed control of interior permanent magnet synchronous motor drive for the flux-weakening operation," *IEEE Trans. Ind. Appl.*, vol. 33, no. 1, pp. 43–48, 1997.

[3] Z. Q. Zhu, Y. S. Chen, and D. Howe, "Iron loss in permanent magnet brushless AC machines under maximum torque per ampere and flux weakening control," *IEEE Trans. Magn.*, vol. 38, no. 5, pp. 3285–3287, Sep. 2002.

[4] J. M. Kim, T. Sun, S. H. Lee, D. J. Kim, and J. P. Hong, "Evaluation and improved design about acoustic noise and vibration in IPMSM," in *Proc. Int. Conf. Electr. Mach. Syst.*, 2010, pp. 1256–1259.

[5] G. Jiao and C. D. Rahn, "Field weakening for radial force reduction in brushless permanent magnet DC motors," *IEEE Trans. Magn.*, vol. 40, no. 5, pp. 3286–3292, Sep. 2004.

[6] G. H. Jang, J. W. Yoon, N. Y. Park, and S. M. Jang, "Torque and unbalanced magnetic force in a rotational asymmetric brushless DC motors," *IEEE Trans. Magn.*, vol. 32, no. 5, pp. 5157–5159, Sep. 1996.

[7] S. D. Garvey, "The vibrational behaviour of laminated components in electrical machines," in *Proc. Int. Conf. Electr. Mach. Drives*, 1989, pp. 226–231.

[8] N. E. Dowling, *Mechanical Behavior of Materials*, 3rd ed. Upper Saddle River, NJ: Prentice-Hall, 2007.